

# Modifying Self-Sensing Circuit To Increase Stability Of Vibration Control

Jeffrey Hodgkins<sup>1</sup>, David Mascarenas<sup>2</sup>, Garnett Simmers Jr.<sup>3</sup>

<sup>1</sup>Department of Mechanical Engineering, University of Massachusetts Lowell, Lowell, Ma 01854

<sup>2</sup>Department of Mechanical Engineering, Colorado State University, Fort Collins, Co 80523

<sup>3</sup>Department of Mechanical Engineering, Virginia Polytechnic Institute and State University, Blacksburg, VA 24061

## ABSTRACT

A single piezoelectric element can be simultaneously used as a sensor and actuator forming a concept of self-sensing actuation. A specially designed electric circuit, referred to as a bridge circuit, is required to realize the concept. Precise equilibrium of the circuit is; however, extremely difficult because of continuous environmental condition changes. In this study, the effects of an unbalanced bridge circuit were evaluated analytically and experimentally in an attempt to quantify the variations in the piezoelectric capacitance in terms of performances in vibration testing and control. Once the dynamic characteristics of self-sensing actuation were identified and understood, methods for improving the system's performance were developed with the use of capacitors in series and parallel with the piezoelectric patch. The analytical and experimental results clearly indicate that the new design scheme increases the stability of the system.

## NOMENCLATURE

|           |   |                           |                                       |
|-----------|---|---------------------------|---------------------------------------|
| $C_p$     | Lead Zirconate Titanate (PZT) capacitance | $K_{aad}, K_{aa}, K_{ss}$ | Actuator matrix gains                 |
| $C_m$     | Matched capacitance                       | $x1s$                     | Sensor location 1                     |
| $C_{add}$ | Added capacitance                         | $x2s$                     | Sensor location 2                     |
| $C_{eq}$  | Equivalent capacitor                      | $x1a$                     | Actuator location 1                   |
| $C_1$     | Signal conditioner capacitance            | $x2a$                     | Actuator location 2                   |
| $R_1$     | Signal conditioner resistance             | $g$                       | Positive position feedback (PPF) gain |
| $V_s$     | Sensing voltage                           | $w_{nf}$                  | PPF natural frequency                 |
| $V_p$     | PZT Voltage                               | $Z_{nf}$                  | PPF damping ratio                     |
| $V_c$     | Control voltage                           | $\omega$                  | Natural frequency of system           |
| $Z_{eq}$  | Signal conditioner impedance              | $\zeta$                   | Damping ratio of system               |
| $Z_p$     | PZT impedance                             |                           |                                       |
| $Z_m$     | Matched capacitance impedance             |                           |                                       |

## 1.0 INTRODUCTION

A single element of piezoelectric material (PZT) can be used as a self-sensing actuator that has many advantages over two elements of PZT used as separate sensors and actuators. Self-sensing actuator systems are lighter and less costly than non-collocated sensor/actuator systems because they employ only one piezoelectric element [1]. Other advantages of self-sensing actuators include: the collocation of sensing and actuation, that allows for the application of a control signal to the point of measured response as well as eliminating capacitive coupling between the sensor and actuator elements [2]. Collocated feedback is also unconditionally stable if there is no adverse effect from actuators [3].

For all of the positive aspects of using a piezoelectric material as a self-sensing actuator, there are some difficulties that have limited the commercial acceptance of piezoelectric self-sensing actuators. First of all, the capacitance of PZT is temperature sensitive, and therefore varies significantly as temperature changes. When used as an actuator, the applied voltage in the piezoelectric material tends to be several times greater than the sensing voltage [1]. Since both signals occur simultaneously in the material, it becomes very difficult to distinguish the sensor voltage from the mixed signals [4]. Bridge circuits (Figure 1.1) [2] are the most popular way to separate the control and sensing signals, but herein lies an even greater challenge. Most balanced bridge circuits use a “dummy” sensor to compensate for changes in environmental conditions such as temperature changes. The downside of a self-sensing actuator circuit is the fact that there is no other piece of piezoelectric material to act as a “dummy” sensor to counteract the changes in capacitance within the material caused by changes in temperature. Therefore, piezoelectric materials used as self-sensing actuators can lead to control stability problems if the environmental conditions are not matched to the properties of the piezoelectric material [1].

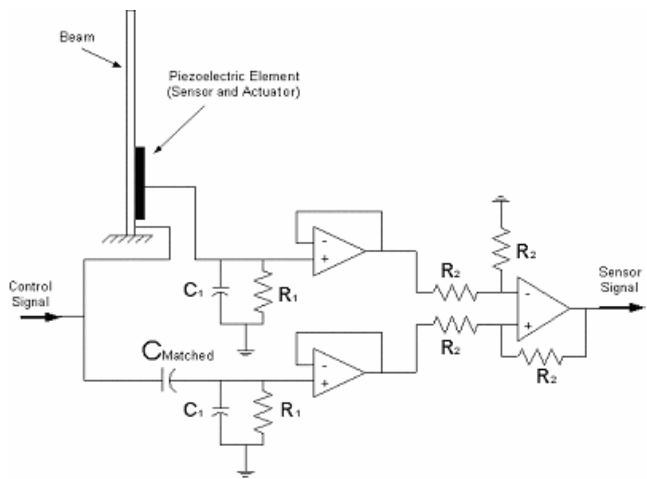


**Figure 1.1: Self-Sensing Actuator Bridge Circuit**

In this paper, the effects of the unbalanced bridge circuit are analytically evaluated in an attempt to quantify the variations in the piezoelectric capacitance as a result of temperature changes. No study has ever been performed to quantify this effect. Once the dynamic characteristics of the circuit were identified, a new design scheme for PZT self-sensing actuation was established to minimize the effect of variations in PZT capacitance caused by temperature changes. The new design includes adding a capacitor in series or parallel with the PZT and matched capacitance. It has been found that the added capacitors increase the system stability while retaining the effectiveness of vibration reduction. Experiments were performed to validate the new design concept. Finally, future issues are summarized for more effective implementation of the new self-sensing design.

## 2.0 CIRCUIT AND STRUCTURE MODELING

### 2.1 Bridge Circuit

In order to utilize self-sensing and actuation of piezoelectric material, a separation of the control voltage supplied to the PZT for actuation and the sensing voltage created by the material’s deformation is necessary. This separation of voltage is performed with a bridge circuit [2]. PZT can be thought of as a voltage source and capacitor ( $C_p$ ) in series [1], resulting in a bridge circuit that is balanced with a capacitor of matched capacitance ( $C_m$ ). There is a difficulty in balancing the bridge circuit attributable to changes in capacitance caused by temperature variations. The PZT used in the experimentation was 5A material that has a trend of one percent change in capacitance to every 5.5 degree C change from room temperature. Figure 2.1 illustrates this trend.

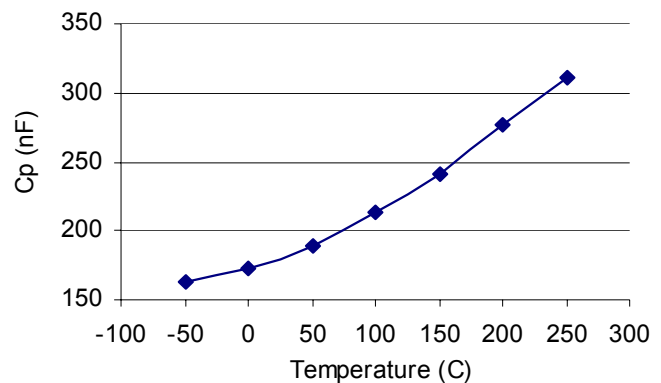


**Figure 2.1: PZT Capacitance (5A) vs. Temperature ( $d_{31}$  data supplied by Piezo Systems, Piezo.com)**

In order to find a useful temperature range for ‘5A’ material an experimental and analytical model of Figure 1.1 were constructed. The experimental model consisted of a 6061-T6 aluminum cantilever beam with two mounted PZT patches. This structure will be discussed further in Section 4. A self-sensing bridge circuit was constructed

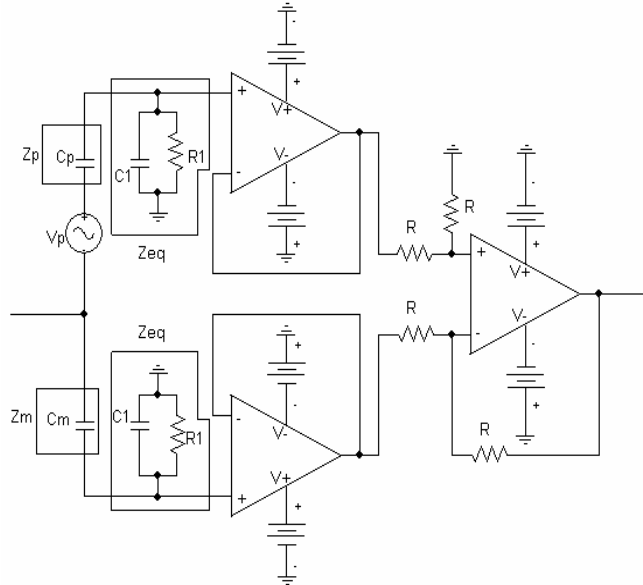


**Figure 2.3: Wiring Diagram of Self-Sensing Circuit**

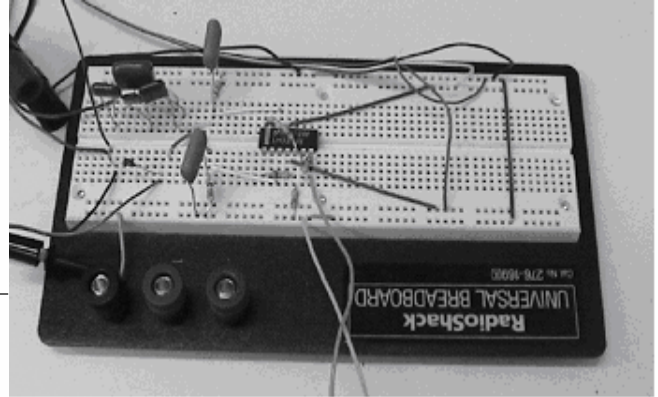


**Figure 2.2: Actual self-sensing circuit**

on a breadboard to allow for easy replacement of the matched capacitor for experimental purposes. Figures 2.2 and 2.3 show the actual circuit used and its wiring diagram representation.

## 2.2 Analytical Model

The analytical model was constructed as a block diagram in MATLAB® Simulink® using the state-space representation of the piezo-beam interaction and the system transfer functions for the circuit components. Figure 2.4 illustrates the Simulink® block diagram of the system.

In the Simulink® block diagram the matrix gains  $K_{aad}$  and  $K_{aa}$  were used to convert the input voltages from the disturbance source and controller into mechanical disturbances that are modified by the dynamics of the system. A state-space block was created to capture the dynamics of the piezo-beam system. The matrix gain  $K_{ss}$  was used to convert the mechanical disturbance back into a voltage output. The values for these four blocks were calculated based upon piezoelectric constitutive and dynamic beam equations. The first four modes of vibration were investigated.

In figure 2.4, the three CP boxes represent the system transfer functions for the upper portion of the bridge circuit containing the contribution of  $C_p$ . The CM box represents the system transfer function of the lower portion of the circuit containing the contribution of  $C_m$ . Equations 2.1 through 2.3 show how these transfer functions were constructed using the voltage loop method and Laplace transforms of Figure 2.3.

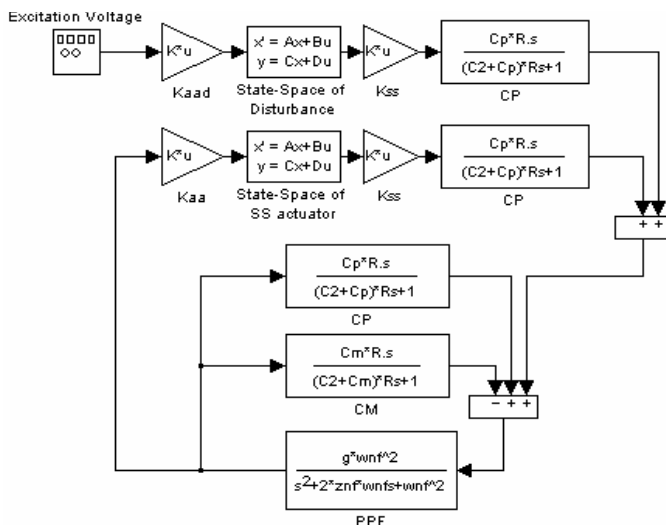


**Figure 2.4: Analytical Block Diagram of System**

$$Z_p = \frac{1}{C_p \cdot s}, \quad Z_m = \frac{1}{C_m \cdot s}, \quad Z_{eq} = \frac{R_1}{C_1 \cdot R \cdot s + 1} \quad (2.1)$$

$$V_s = \frac{Z_{eq}}{Z_{eq} + Z_p} V_c - \frac{Z_{eq}}{Z_{eq} + Z_m} V_c + \frac{Z_{eq}}{Z_{eq} + Z_p} V_p \quad (2.2)$$

$$V_s = \frac{C_p \cdot R \cdot s}{R(C_1 \cdot s + C_p \cdot s) + 1} V_c - \frac{C_m \cdot R \cdot s}{R(C_1 \cdot s + C_m \cdot s) + 1} V_c + \frac{C_p \cdot R \cdot s}{R(C_1 \cdot s + C_p \cdot s) + 1} V_p \quad (2.3)$$

Equation 2.3 shows that if the value of  $C_p$  is equal to  $C_m$ , the bridge circuit is balanced and the resulting output voltage will be the sensing voltage ( $V_p$ ). If  $C_m$  is not equal to  $C_p$ , a portion of  $V_c$  is superimposed

with  $V_p$ , resulting in potential instability. This phenomenon of circuit unbalance has been observed in many cases [1].

The PPF block represents the positive position feedback (PPF) controller used in the actual experiment to create a vibration reduction when the system was subjected to disturbance. The equation seen in the PPF block of Figure 2.4 is the basic equation for this type of controller, the values of  $g$ ,  $\omega_{nf}$ , and  $z_{nf}$  are values that are obtained using a trial-and-error approach during the experimental stage [5].

### 2.3 Analytical Observations

Before any experimental data was taken, analytical simulations were performed to study the reaction of the system to an unbalanced bridge circuit. With the PPF controller disconnected from the rest of the analytical model, frequency response functions (FRF) of the entire beam/circuit system were taken. The value for  $C_p$  was changed to observe the effect of the unbalanced bridge circuit on the FRF.

A change in resonant and anti-resonant locations in the FRF was observed. With a value of  $C_p$  less than  $C_m$ , the anti-resonance appears before the resonance and the opposite would occur when  $C_p$  was greater than  $C_m$ . However, when the value of  $C_p$  became balanced with  $C_m$ , the anti-resonance disappears. Figure 2.5 illustrates the change in FRFs as a result of  $C_p$  perturbations.

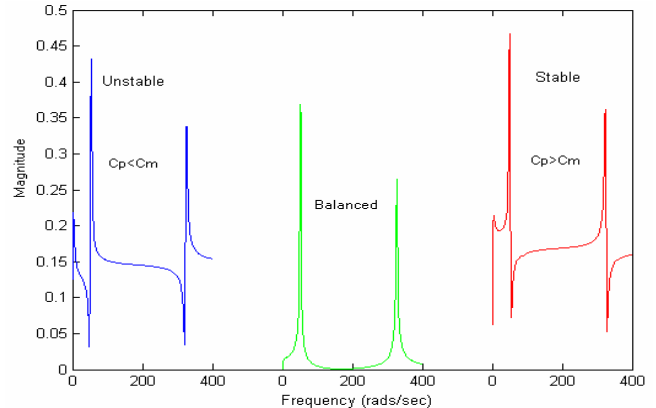


Figure 2.5: Changes in FRF vs. Cp Value

This change in resonant and anti-resonant peaks has been observed to affect the PPF controller's ability to stabilize the system. When the resonance occurred before the anti-resonance, the analytical model became unstable when the PPF controller was activated, and when the anti-resonance occurred before the resonance, the system would remain stable and vibration reduction would occur. However, when the value of  $C_p$  became increasingly smaller than  $C_m$  the effectiveness of the vibration control to decrease to the point where there was no apparent reduction. Figure 2.6 demonstrates the relationship between  $C_p$  and  $C_m$  relative to control stability.

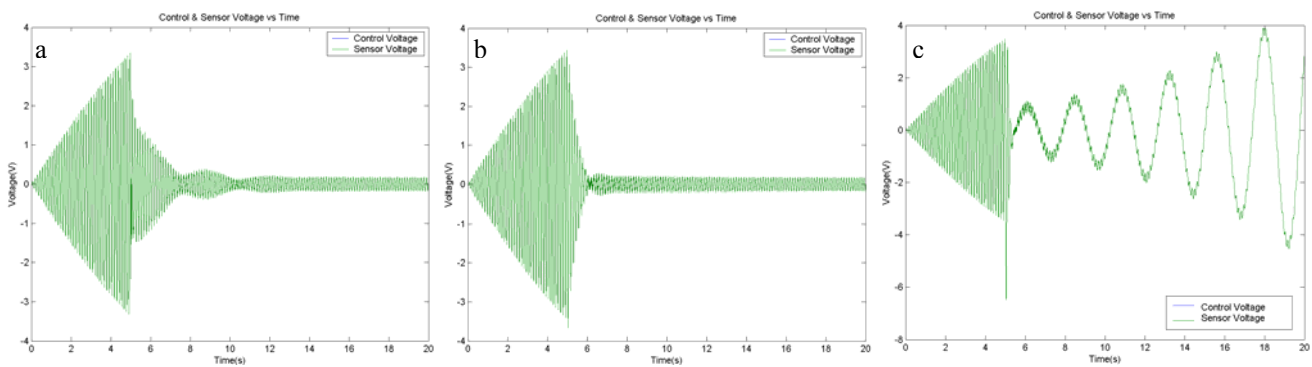
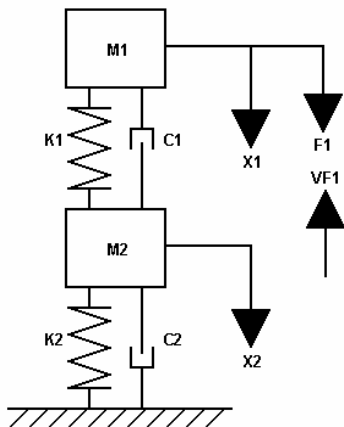


Figure 2.6: Affect of  $C_p$  on PPF Control  
 a)  $C_p = 0.9C_m$ , b)  $C_p = C_m$ , c)  $C_p = 1.06C_m$

In order to quantify the cause of this instability, a two degree of freedom (DOF) 'self-sensing system' was constructed and a stability analysis was performed. The 2 DOF system can be seen in Figure 2.7. A force,  $F_1$ , representing the control voltage  $V_c$  is applied to the first DOF and the response of that DOF,  $X_1$ , represents the sensor voltage,  $V_p$ . A force  $VF_1$ , equivalent to the voltage across the matched capacitor is applied in the direction opposite to  $F_1$ . Therefore, if  $VF_1$  and  $F_1$  are of the same value, they will cancel each other out and only  $V_p$  will remain. If  $F_1$  is higher than  $VF_1$  than the resultant output will be  $X_1 + \Delta F_1$  which represents the case where  $C_p < C_m$  following the voltage law  $V = q/C$ . In the experimental system, this case will create a stable system; however, since the experimental system is controlled with PPF, the resulting control will be unstable. The exact

opposite occurs when  $F1$  is at a lesser value than  $VF1$  ( $C_p > C_m$ ), and the 2 DOF system becomes unstable. Figure 2.8 illustrates the case of stability, perfect balance, and instability of the 2 DOF system. The conclusions reached from this analysis validate the assumptions reached from the analysis performed above.



**Figure 2.7: Mechanical Equivalent of Self-Sensing Circuit**

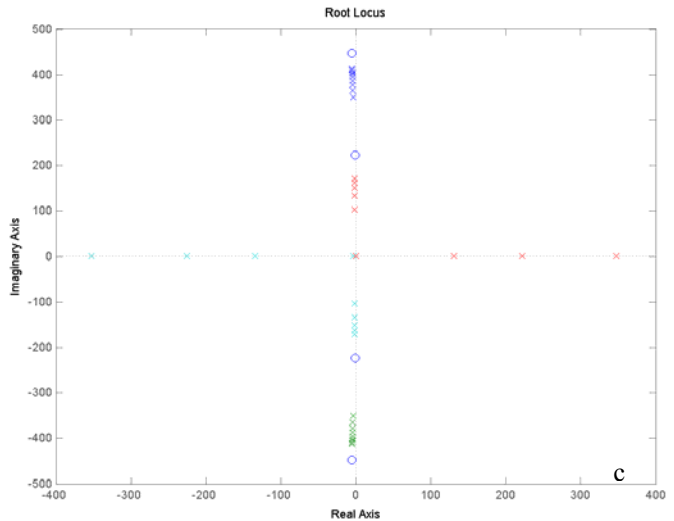
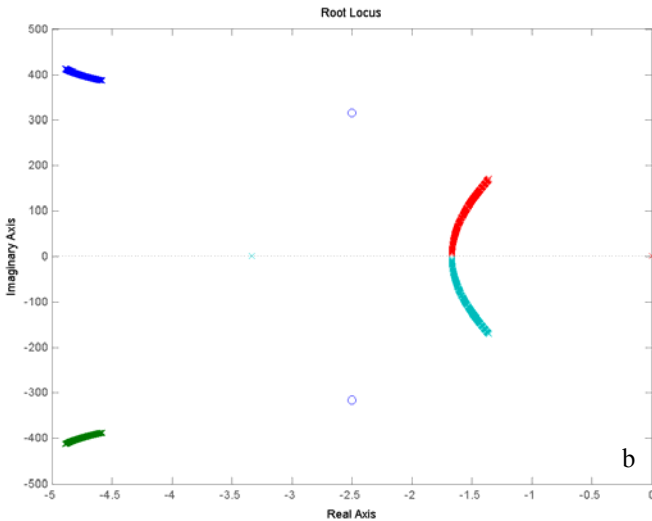
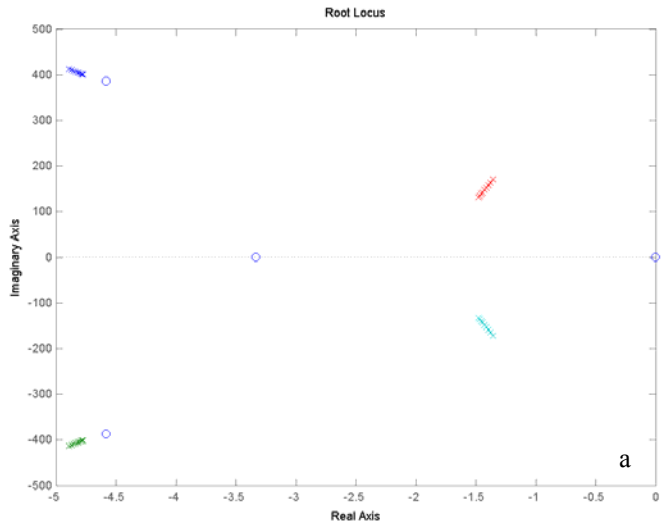


**Figure 2.8: Affect of  $C_p$  on PPF Control**  
a)  $C_p > C_m$ , b)  $C_p = C_m$ , c)  $C_p < C_m$

### 3.0 INCREASING THE STABILITY OF THE SELF-SENSING CIRCUIT

#### 3.1 Proposed Modifications

There are two proposed modifications to the self-sensing circuit that could improve the stability of the system. Adding a capacitor in series or parallel with the PZT capacitance ( $C_p$ ) and the matched capacitance ( $C_m$ ) should increase the stability of the self-sensing circuit. Both modifications are based on the idea that adding capacitance to the circuit would change the equivalent capacitance in such a way that a temperature disturbance in the PZT patch would produce a smaller change in the capacitance mismatching between  $C_p$  and  $C_m$ .

#### 3.2 A Theoretical Case for Adding Capacitors

A theoretical example will be used to illustrate the point of added capacitance. Assume that in the self-sensing circuit  $C_p$  and  $C_m$  are equal to 100 nF. It will also be assumed that there is a temperature change that produces a 5 nF increase in the capacitance of  $C_p$ . In the case were there is no added capacitance, this change creates a 5% difference in matching between  $C_p$  and  $C_m$ . We will assume that a 5% mismatch leads to instability.

The theoretical circuit will now be modified by placing an added capacitor ( $C_{add}$ ) of 100 nF in parallel with  $C_p$  and  $C_m$ . In this scenario, the 5 nF disturbance in  $C_p$  will not produce the same percentage mismatch between  $C_p$  and  $C_m$  because the parallel addition of  $C_{add}$  changes the equivalent capacitance ( $C_{eq}$ ) according to Equation 3.1.

$$C_{eq} = C_{add} + C_p \quad (3.1)$$

A disturbance equivalent to the first example now only produces a 2.5% mismatch between  $C_p$  and  $C_m$ . A similar example can be arranged for the addition for  $C_{add}$  in series with  $C_p$  and  $C_m$ . The equivalent capacitance changes according to Equation 3.2 and a 5 nF temperature disturbance in  $C_p$  creates a 2.4% mismatch between  $C_p$  and  $C_m$ .

$$C_{eq} = \frac{1}{\left(\frac{1}{C_{add}}\right) + \left(\frac{1}{C_p}\right)} \quad (3.2)$$

Therefore, both of the modified circuits are stable even though they experience the same temperature induced change in  $C_p$  that drove the first system unstable.

### 3.3 Analytical Modeling of Added Capacitance

The addition of series and parallel capacitors to the self-sensing circuit were modeled analytically because the previous scenarios are oversimplified to account for the true effects on the circuit. The PZT patch attached to the structure acts as a voltage source and capacitance. Adding capacitance to the self-sensing circuit will change the circuit dynamics. Therefore the transfer functions used within the Simulink® models had to be adjusted for this change in system impedance.

Equation 3.4 shows the transfer function for the added series capacitor and Equation 3.5 depicts the transfer function for the added parallel capacitor.

$$V_s = \frac{C_{add} \cdot C_p \cdot R_1 \cdot s}{(C_1 \cdot (C_{add} + C_p) + C_{add} \cdot C_p) R_1 \cdot s + C_{add} + C_p} \cdot V_c - \frac{C_{add} \cdot C_{p21} \cdot R_1 \cdot s}{(C_1 \cdot (C_{add} + C_{p21}) + C_{add} \cdot C_{p21}) R_1 \cdot s + C_{add} + C_{p21}} \cdot V_c + \frac{C_{add} \cdot C_p \cdot R_1 \cdot s}{(C_1 \cdot (C_{add} + C_p) + C_{add} \cdot C_p) R_1 \cdot s + C_{add} + C_p} \cdot V_p \quad (3.4)$$

$$V_s = \frac{(C_{add} + C_p) \cdot R_1 \cdot s}{(C_1 + C_{add} + C_p) R_1 \cdot s + 1} \cdot V_c - \frac{(C_{add} + C_{p21}) \cdot R_1 \cdot s}{(C_1 + C_{add} + C_{p21}) R_1 \cdot s + 1} \cdot V_c + \frac{(C_{add} + C_p) \cdot R_1 \cdot s}{(C_1 + C_{add} + C_p) R_1 \cdot s + 1} \cdot V_c \quad (3.5)$$

The positive position feedback (PPF) parameters were held constant for the analytical simulation as in the previous case. It should be noted that the PPF parameters might have to be varied to alter performance during the experimental verification. The value of  $C_p$  was set equal to  $C_m$  at 21.1 °C to simulate an experiment at room temperature with 5A PZT material.

### 3.4 Analytical Results

The results of the analytical simulation in Figure 3.1 indicate that the added series and parallel capacitors should increase stability. With no added capacitance the system was stable until  $C_p$  was 5% greater than  $C_m$ , and when  $C_p$  was 10% less than  $C_m$  the settling time ( $t_s$ ) was 1.25 s. A series added capacitor equal to the value of  $C_m$  remains stable until  $C_p$  was 15% greater than  $C_m$ , but when  $C_p$  was 10% less than  $C_m$  the settling time increased to 5.05 s. A parallel-added capacitor equal to  $C_m$  remained stable till  $C_p$  was 9% greater than  $C_m$ , and the settling time increased to 2.40 s.

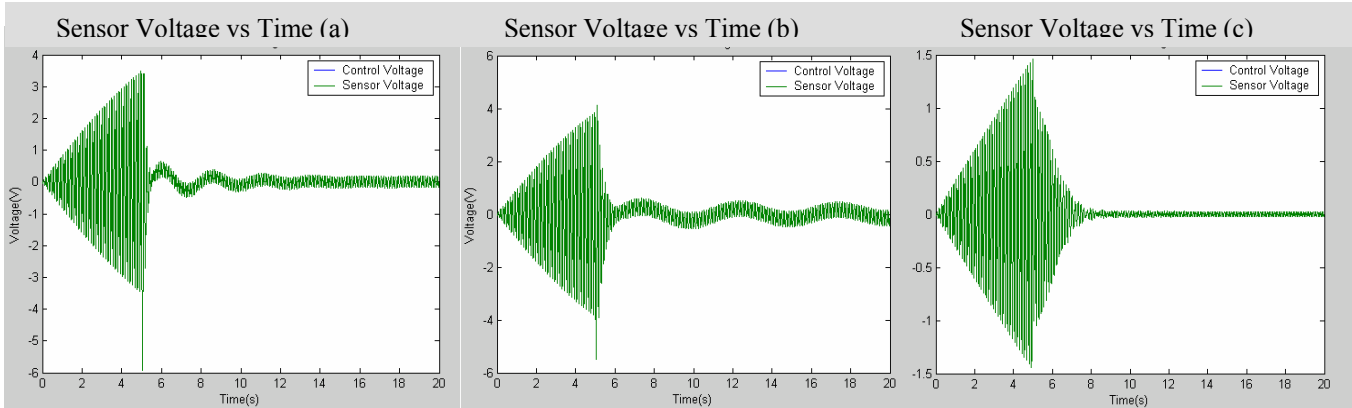


**Figure 3.1: Stability Thresholds for Three Cases**  
a)No added capacitance at 5%, b)Parallel case 9%, c)Series 15%

In the simulation, a 1% increase in  $C_p$  is equivalent to a 5.5 degree Celsius increase in temperature for 5A PZT material. Thus, a parallel addition will increase stability an additional 22 °C change in temperature, and a series addition will increase stability an additional 55 °C change in temperature. The downside is that the series settling time increased by 304% and the parallel settling time increase 92%. It should be noted that the gains remained constant for the experiment. As a result of increase in stability, it would be possible in the experimental case to increase the gain, which would reduce the settling times. The trade-off would be increased stability at the cost of increased power to the actuator.

## 4.0 EXPERIMENTAL VERIFICATION

### 4.1 Experimental Setup

An angle iron bracket was bolted to a square sheet of aluminum (.355 mx.311 mx.005 m) that served as the base of the structure. Two pieces of 5A PZT material were mounted to a cantilever beam, and the beam was clamped to the angle iron bracket. As a result of unexpected grounding issues, only the root patch was utilized experimentation. Thus, the vibration disturbance and self-sensing actuation were handled with the root PZT patch. A picture of the structure can be seen in Figure 4.1, and Table 4.1 contains the important dimensions and specifications for the structure.

**Table 4.1: Cantilever beam data**

|                             |              |
|-----------------------------|--------------|
| Length                      | 0.398m       |
| Width                       | 0.190m       |
| Thickness                   | 0.00158m     |
| Distance from root to patch | 0.0180m      |
| Length of root patch        | 0.072        |
| Distance between patches    | 0.045        |
| Length of patch 2           | 0.072        |
| E                           | 6.90E+10     |
| Base                        | 0.335x0.311m |
| Base thickness              | 0.005        |

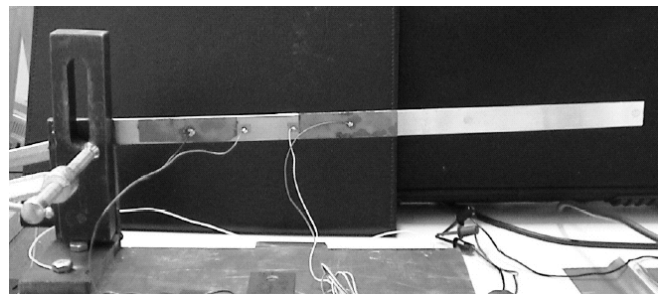


**Figure 4.1: Cantilever beam structure with PZT**

A self-sensing circuit [2] was assembled on a circuit board, and the op-amps were powered by a Calnex® dual source DC power supply. A Dactron® SPECTRABOOK® was used for data acquisition and to supply chirp and sine disturbance inputs to the structure. A PCB® 790 inverting power amplifier, specifically designed for use with PZT, amplified the source voltage and current.

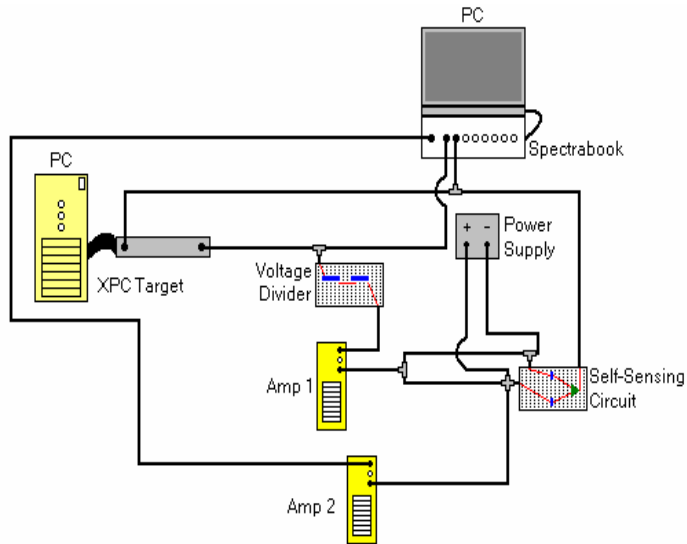


**Figure 4.2: System diagram minus the structure**

The PPF control was built in Simulink® and a MATLAB® script was written to supply the PPF parameters to the Simulink® code. The Simulink® code of the PPF control was implemented with a National Instruments® 2345 data acquisition board with an XPC Target® card. The control output was amplified by a PCB® 790 amplifier and then routed to the self-sensing circuit. A diagram of the complete system (minus the structure) can be seen in Figure 4.2.

#### 4.2 Dealing With Saturation

Initial attempts to unbalance the system failed because of voltage saturation. The XPC card is limited to an output and input voltage of only ten volts, so a saturation block was employed in the Simulink® code to protect the XPC card from potential overload. As it turns out, the saturation block always makes the system stable because the PPF is limited to the

current supplied by the 10 volt output. For the structure tested, the power associated with a 10 volt output is not large enough to drive the system unstable. The saturation problem was modeled analytically to confirm that the system would always be stable. This problem had to be solved because it was necessary to drive the system unstable so the analytical predictions could be tested. To allow for better data correlation, the Simulink® model was modified to take the saturation issues into consideration.

A voltage divider circuit was used solve the saturation problem. A twenty to one divider was created to protect the XPC circuit while allowing the PPF to output more power and contribute to the beam's dynamics. This modification solved the saturation problem, and it allowed for the experimental validation of the analytical results. Precise balance of the bridge circuit was challenging in the beginning because temperature and bonding condition changes can affect the results by changing the PZT capacitance ( $C_p$ ). Care was taken to perform the experiment quickly to ensure the temperature remained constant throughout all of the individual trials. The  $C_p$  and matched capacitance ( $C_m$ ) were matched at the start of each experimental session.

#### 4.3 Frequency Response Functions

Frequency response functions (FRFs) were measured for increasing and decreasing the values of  $C_m$ . When  $C_m$  was less than  $C_p$  the FRFs showed poles occurring before zeros. When  $C_m$  was greater than  $C_p$ , the zeros preceded the poles. When the capacitances were matched the zeros were not seen in the FRF because of small magnitudes could only be seen by using a semi-log scale. The resonant/antiresonant patterns seen in the experimental FRFs match those predicted by the analytical FRFs.

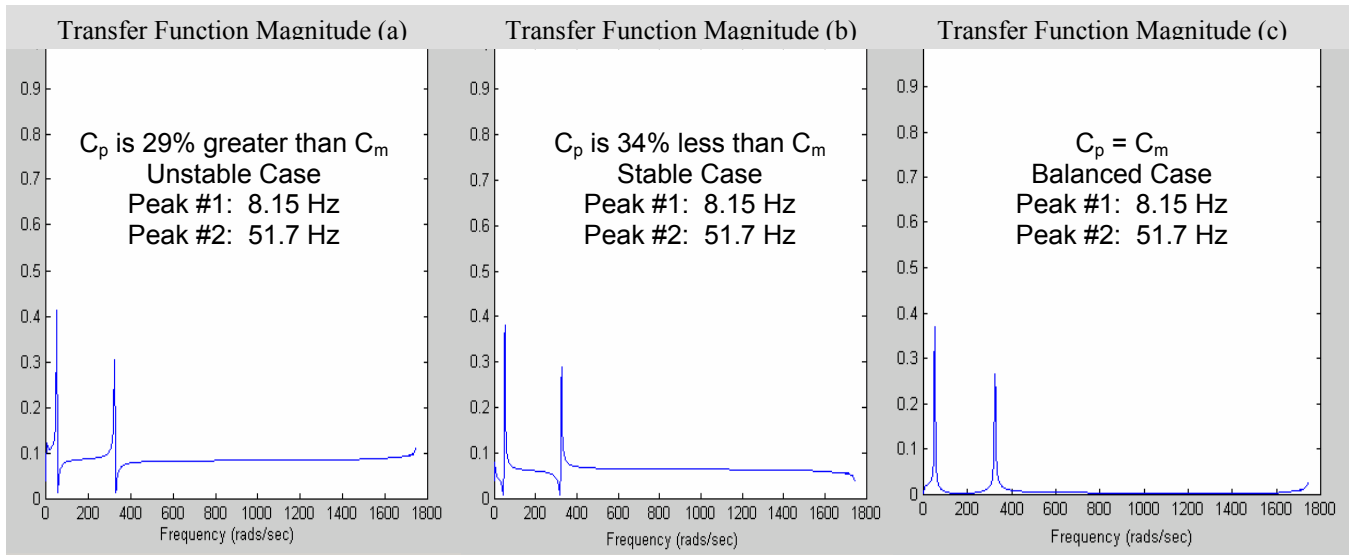


**Figure 4.3: Experimental FRFs**

The magnitude change in the FRF can be explained using the transfer function for the bridge circuit. The frequency response function is a measure of the output divided by the input. The input is a 0-300 Hz chirp signal supplied by the Dactron. The output is the sensing voltage represented by Equation 2.3. When  $C_p=C_m$  the  $V_s$  is directly proportional to  $V_p$ , but when  $C_p \neq C_m$ , part of the sensing voltage depends on  $V_c$ . This increases or decreases the output, thus the magnitude shifts.

#### 4.4 Stability and Effectiveness Results

After the FRF data was collected the values of  $C_p$  and  $C_m$  were measured, and adjustments were made to ensure matching. All additional capacitors added ( $C_{add}$ ) to the system were equal to  $C_p$  at 21.1 °C. All PPF parameters were held constant during the testing. The system was tested in the matched case for the following conditions: no added capacitor, a series added capacitor, and a parallel added capacitor. All three systems were tested with no capacitance disturbance caused by a temperature change. Figure 4.3 shows that with no disturbance the no added, series added, and parallel added capacitor cases were all stable.

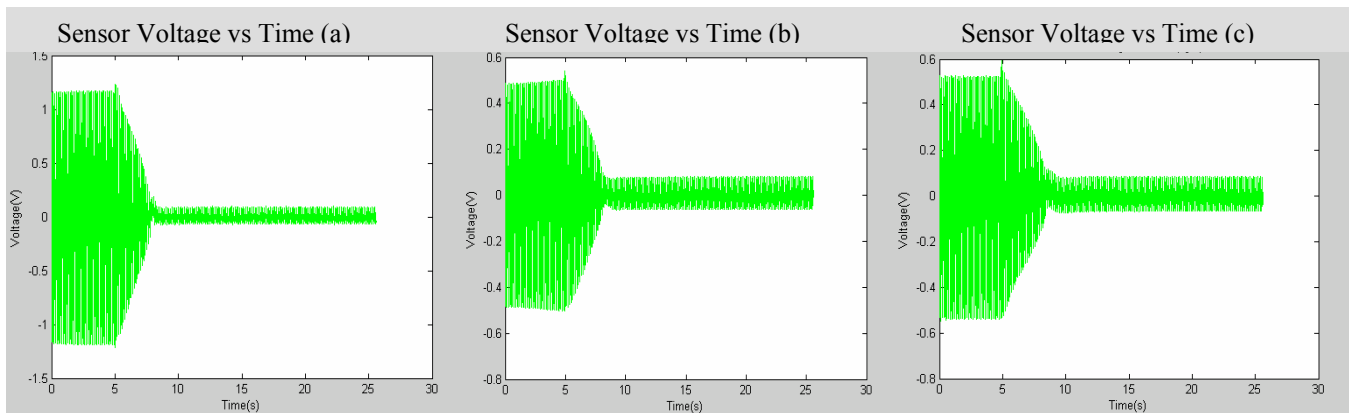


**Figure 4.4: Sensor voltage vs time for no temperature disturbance**

a) no added capacitors b) series added capacitors c) parallel added capacitors

A second group of tests were conducted for a simulated temperature change. A temperature disturbance was experimentally tested by adding a 4 nF capacitor in parallel with the PZT or the matched capacitor. Figure 4.4 shows the results of the tests when the 4 nF disturbance was added to the  $C_p$ . The no added capacitor case was unstable, but the series and parallel added capacitor cases remained stable.

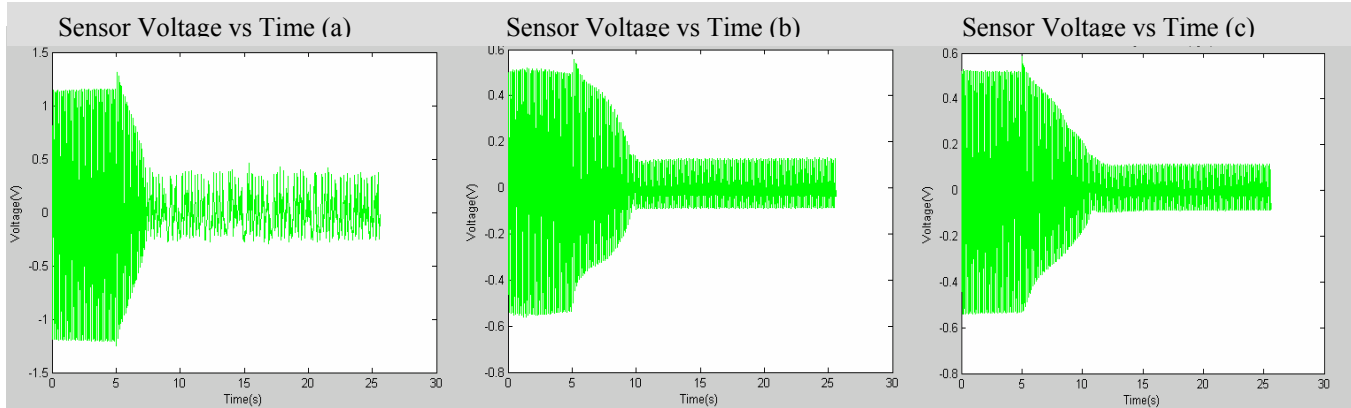


**Figure 4.5: Sensor voltage vs time plots for a 4 nF disturbance caused by a temperature change.**  
 a) no added capacitors b) series added capacitors c)parallel added capacitors

A third series of tests were conducted to simulate an even larger temperature change. A 10 nF disturbance was added to the circuit in various configurations to simulate a large temperature change. Figure 4.5 shows the results of these tests when the disturbance has added to  $C_p$ . In this case, only the circuit with the parallel added capacitance was still stable.

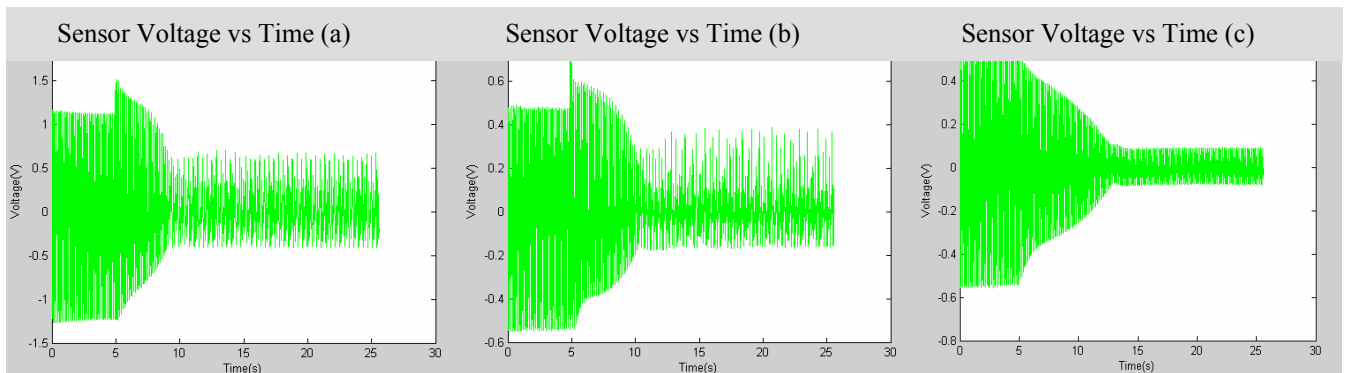


**Figure 4.6: Sensor voltage vs time plots for a 10 nF disturbance caused by a temperature change.**  
 a) no added capacitors b) series added capacitors c)parallel added capacitors

The experimental tests show that adding series and parallel capacitances to the self-sensing circuit can increase stability. The results also show that adding capacitors increases the settling time/effectiveness (see Table 4.2). This happens because the capacitors absorb energy like springs in mechanical systems, which decreases the sensing and applied voltage. This has the effect of changing the dynamic range of the PZT sensor, thus the ability to sense a disturbance decreases. If a disturbance is not sensed then it cannot be controlled through actuation.

**Table4.2: Experimental results**

|  | Stable    | Settling |
|--|-----------|----------|
|  | Condition | Time (s) |
| $C_p=C_m$ w no $C_{add}$               | yes       | 2.81     |
| $C_p=C_m$ w Series $C_{add}$           | yes       | 3.46     |
| $C_p=C_m$ w Parallel $C_{add}$         | yes       | 3.35     |
| $C_p=C_m$ wo $C_{add}+4$ Nf            | no        | N/A      |
| $C_p=C_m$ w Series $C_{add}+4$ nF      | yes       | 6.08     |
| $C_p=C_m$ w Parallel $C_{add} + 4$ nF  | yes       | 5.03     |
| $C_p=C_m$ wo $C_{add}+10$ nF           | no        | N/A      |
| $C_p=C_m$ w Series $C_{add}+10$ nF     | no        | N/A      |
| $C_p=C_m$ w Parallel $C_{add} + 10$ nF | yes       | 7.70     |

A final experimental test was conducted for the parallel case in an attempt to increase effectiveness while retaining increased stability. The voltage divider circuit was modified to have a 12 to 1 voltage split. This was done to increase the power to the PZT for control actuation. Figure 4.6 shows the settling time decreased from 7.70 s to 2.03 s when a 10 nF disturbance was added to  $C_m$ . When the 10 nF disturbance was added to the  $C_p$  the system stability was inconclusive. This could mean that there is a tradeoff between increased stability and effectiveness.

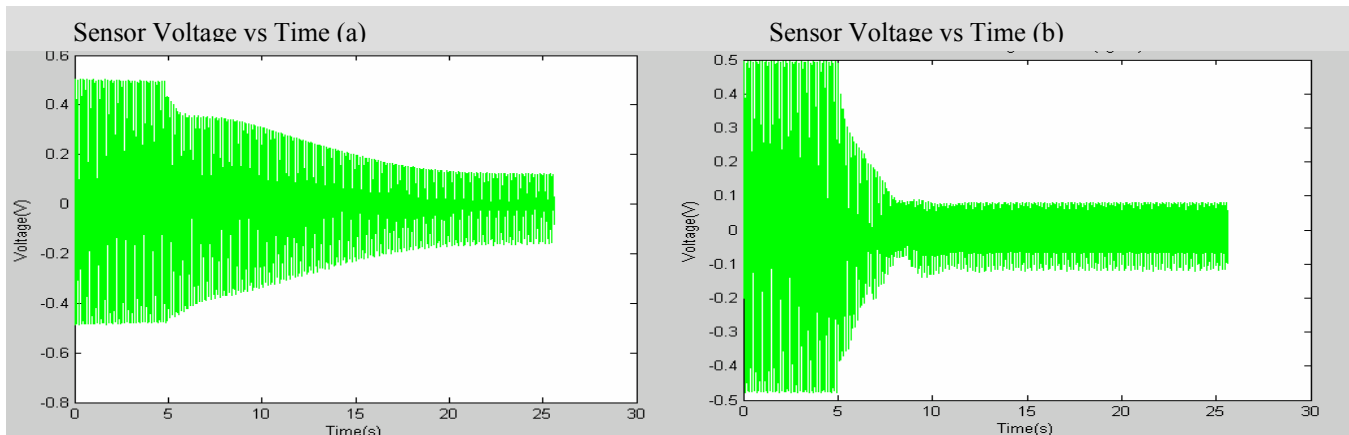


**Figure 4.6: Shows that vibration reduction increases as the power to the controller increases**  
a) with a 20 to 1 voltage split b) with a 12 to 1 voltage split

## 5.0 DISCUSSION

### 5.1 No added capacitance

This study has focused on identifying the usable temperature range of the piezoelectric material PZT 5A. A cantilever beam structure using PZT as a self-sensing actuator was constructed. An analytical model of the self-sensing actuation system was created using MATLAB® Simulink®. The results from this analytical model (with no added capacitor) show that an increase in  $C_p$  by 4% or 22 °C from room temperature will continue to provide a balanced bridge circuit and allow for effective vibration control. In analytical model observations, the positive position feedback controller could not create a stable system if  $C_p$  was equal to or exceeded a 5% increase from room temperature capacitance. Experimentally, with no added capacitance, when  $C_p$  was increased 4.19% (4nF) the system went unstable.

### 5.2 Added parallel capacitance

The analytical model was modified to facilitate a capacitor placed in parallel with the PZT capacitance and the matched capacitance. The analytical model predicted that the system would remain stable up to the point where  $C_p$  exceeded  $C_m$  by 9%. When  $C_p$  was 10% greater than  $C_m$  the system went unstable.

In the experimental case, when  $C_p$  was increased by 10.5 % (10 nF) beyond  $C_m$  the system was stable. This shows that an added capacitor placed in parallel with  $C_p$  and  $C_m$  increased stability by 6.3% (6 nF). This means the system will remain stable for an increase of 35 °C beyond the point where the system with no added parallel capacitor went unstable.

### 5.3 Added series capacitance

The analytical model was also modified to facilitate a capacitor placed in series with  $C_p$  and  $C_m$ . An increase in stability was also observed. A 13 % increase in PZT capacitance beyond room temperature was a result of the added series capacitor while still allowing for stable vibration reduction.

Along with the parallel capacitance experiments, the series tests were not performed to find the limits of stability as a result of added capacitance. These tests were performed to show increased stability over the case with no added capacitors. The series capacitor stabilized the 4.19% (4 nF) increase in  $C_p$ , as did the parallel capacitor, but was unable to fully control the 10.5% (10nF) increase. Thus, the series added capacitor did increase stability

because it stabilized a 4 nF disturbance that the original circuit could not stabilize. The 10 nF disturbance test was inconclusive. The limit of the stability increase attributed to the series capacitor addition most likely lies between those two disturbance values.

#### **5.4 Settling time**

The downside of adding capacitance in series and parallel seems to be the effect on settling time when  $C_m$  is greater than  $C_p$  (a stable case that causes the controller to be ineffective in vibration reduction). When a capacitor is added in parallel or in series to  $C_p$  and  $C_m$ , the applied voltage drops. The reduction in the applied signal causes the system to damp out vibrations more slowly. In the experimental case, this increase in settling time could be offset by increasing the power to the PPF, but it was unclear how this would affect stability. It could be that there is a tradeoff between stability and effectiveness that could be optimized based on the amount of reduction desired and the change in temperature the system will experience.

### **6.0 CONCLUSIONS**

The dynamic characteristics of self-sensing actuation were quantified for the first time in literature. Two new design schemes (adding series or parallel capacitors to  $C_m$  and  $C_p$ ) have been used to increase control stability, which makes self-sensing actuation more commercially viable. The effectiveness of the two design schemes can be enhanced at the cost of increased power to the controller. Both new design schemes were validated experimentally and shown to improve system performance with respect to temperature resistance.

### **7.0 RECOMMENDATIONS**

Several elements of the system contributed to the complications and difficulty in system's assessment of stability. The environment in which the structure was set in during experimentation was not a controlled environment and would vary in temperature by as much as 6 °C. A temperature-controlled environment would reduce the possibility of changing the PZT patch's capacitance. Bonding constraints of the PZT to the aluminum beam was a variable that could not be quantified. If the bonding was not ideal anywhere along the patch, the capacitance could contribute additional changes in capacitance. Further studies on inspecting PZT bonding and frequency dependence are necessary.

A difficulty in distinguishing ineffectiveness and instability was a result of the voltage saturation implemented into the system to protect the XPC Target® controller as well as the Dactron® SPECTRABOOK® from voltage overload, which in turn limited the amount of power available for the PPF controller to use for stabilization. Further study in power usage is necessary in order to fully demonstrate the results of stability control.

Further study in optimizing the use of series and parallel capacitors is necessary to create a more robust system. This resulting system should allow for a large range of PZT capacitances caused by temperature changes while still allowing for optimal vibration reduction.

These techniques for self-sensing robustness should be applied to complex and real-scaled structures where damage detection is warranted. Piezoelectric materials excel at detecting damage and controlling structures, but up to this point instability has limited the usefulness of PZT in these applications. A more robust self-sensing circuit should make PZT as a self-sensing actuator more viable for detecting damage and controlling complex structures.

### **8.0 ACKNOWLEDGEMENTS**

The research was conducted at the Los Alamos National Laboratory in Los Alamos, New Mexico as part of the 2003 Dynamic Summer School. The Engineering Science and Applications--Weapons Response Division and The Department of Energy's Education Programs Office, provided funding for this research. Great thanks goes to the following companies for their software donations: MathWorks Inc. (MATLAB®), and Vibrant Technology Inc. (ME'ScopeVES®). The authors would like to acknowledge Henry Sodano for his assistance in the construction and trouble shooting of the experimental self-sensing bridge circuit. The authors would also like to give great thanks to Charles Farrar for organizing the Dynamic Summer School, and their mentors, Gyuhae Park and Hoon Sohn, for their dedication and being valuable resources.

## 9.0 REFERENCES

- [1] Tani J., Cheng G., Qiu J., "Effectiveness and Limits of Self-Sensing Piezoelectric Actuators" Proceedings of 1<sup>st</sup> Structural Health Monitoring Workshop, 1997, pp. 503-514, 1997.
- [2] Dosch J., Inman D., Garcia E., "A Self-Sensing Piezoelectric Actuator for Collocated Control" Journal of Intelligent Material Systems and Structures, Vol. 3 January, pp. 166-185, 1992.
- [3] Goh, C. J. and T. K. Caughey, "On the Stability Problem Caused by Finite Actuator Dynamics in the Control of Large Space Structures", International Journal of Control, Vol. 41 No. 3, pp. 787-802, 1985
- [4] Oshima Kazuhiko, Takigami Tadao, Hayakawa Yoshikazu, "Robust Vibration Control of a Cantilever Beam Using Self-Sensing Actuator" JSME International Journal, Vol. 40 No. 4, pp. 681-687, 1997.
- [5] Poh, S. and A. Baz, 1990, "Active Control of a Flexible Structure Using a Modal Positive Position Feedback Controller", Journal of Intelligent Material Systems and Structures, Vol. 1, July, pp. 273-288.